International Journal of Impact Engineering 104 (2017) 85–94

Contents lists available at ScienceDirect

International Journal of Impact Engineering

journal homepage: www.elsevier.com/locate/ijimpeng

Sand ejecta kinematics and impulse transfer associated with the buried blast loading: A controlled laboratory investigation

Padmanabha Vivek[a,*], Thallak G. Sitharam[b]

[a] Research Scholar, Department of Civil Engineering, Indian Institute of Science, Bangalore, India
[b] Department of Civil Engineering, Indian Institute of Science, Bangalore, India

ARTICLE INFO

Article History:
Received 8 September 2016
Revised 16 December 2016
Accepted 26 February 2017
Available online 28 February 2017

Keywords:
Shock tube
Buried blast
Sand ejecta
Impulse

ABSTRACT

An experimental test facility has been developed for performing laboratory studies on shallow buried blast loading. The shock tube based test facility offers an alternative method for generating blast wave in a controlled and repeatable manner, without the use of explosives. In this paper, we consider a spherical expanding blast wave of moderate shock strength with relatively low driving pressure. A confined dry sand bed prepared with a constant density, is exposed to a blast wave from the embedded shock tube. The principal objective of this paper is to understand the various events involved during the interaction of leading blast wave with the soil medium, followed by the expansion of the entrained gas. The process initiates with the formation of stress wave in the sand media, followed by the gas bubble expansion and terminates with sand ejection. The variation in the output of the sand ejecta is investigated with the help of high speed photography. The velocity of the sand ejecta front is found to decrease with the increase in the burial depth (DoB). Further, the impulse (using vertical pendulum) and peak pressure (using transducers) imparted to the rigid target are evaluated. The target is located at different stand-off distances (SoD) above the top surface of the sand bed. It is found that the peak pressure values are influenced by the presence of dome-cap of the ejecta, expanding vertically upwards generating a point-load impact. Irrespective of the depth of burial (DoB = 32 mm–64 mm), maximum impulse is observed around the zone of bubble expansion (close to the sand bed surface). Sand ejecta does however have a greater influence on the impulse at higher SoDs (> 40 mm). Moreover, the maximum momentum transfer is observed when SoD to DoB ratio is 2.5. In conclusion, the shock-driven sand test facility is found to be a simple and efficient tool to study the complex dynamics of sand ejecta, including the post- impact on the target structures.

1. Introduction

For over a century, ammunitions like improved explosive device (IED) and landmine were commonly used in warfare, causing significant threat to light weight military vehicles and to personal lives onboard [1]. During the past several years, it has become popular among terrorists groups to bury an explosive device few centimeters below the ground surface and cause fatalities of considerable proportion. With an explosion at an optimum buried depth, sand debris is expected to carry maximum momentum over the surface [2]. Researchers have been investigating the problem for a deeper understanding by performing a full scale buried blast test [3–5]. However, physical test involving full scale blasts are very expensive and are not repeatable [6,7]. Numerous authors [8,9,6] have also performed simulated buried blast and surrogate mine experiments using scaled explosive charges. The investigation primarily includes the influence of depth of burial (DoB), soil type, moisture content, height of burial (HoB) and the effect on the target placed at different stand-off distances (SoD) [7,10]. However, very few authors have investigated the soil behavior during buried blast loading. Ambrosini et al. [11] and Roger [12] have performed series of field experiments by using TNT explosives above and below the ground surface. Bergeron et al. [2] performed experiments by using scaled C4 explosive charges. The pressure and arrival time of air-shock (above the surface) and ground-shock (below the surface) were recorded over a range of distances. The shock wave propagation was found to be significant near the source of explosion and found to decelerate with distance. Karinski et al. [13] and Tan et al. [14] carried out numerical simulations predicting the attenuation of stress waves in soil upon a buried explosion.

The output from the buried blast event, peak pressure and impulse are measured by using various techniques. Braid et al. [15] have used pitot tubes to measure the stagnation pressure at close proximity of the air blast. Anderson et al. [10] have used cable-pull

* Corresponding author.
E-mail address: vivek2387@gmail.com (P. Vivek), sitharam@civil.iisc.ernet.in (T.G. Sitharam).

http://dx.doi.org/10.1016/j.ijimpeng.2017.02.017
0734-743X/

potentiometer in their mine blast experiments, the total impulse transferred to the flat plate and V-shaped plate is determined from the maximum height achieved. Pressure transducers (or multiple spike gauges) were also used to measure the peak pressure and impulse [16,17]. McShane et al. [18] conducted series of experiments using Kolsky bar; the initial peak pressure and transient phase were measured from the recorded strain gauge data. Clarke et al. [19] developed a reaction frame with Hopkinson pressure bars. The pressure-time response generated from the large scale (1/4 scale) experiment has been used to generate spatial and temporal loading of an explosion event. A most popular and accurate mode of impulse measurement is done using vertical pendulum apparatus [3,20,7,21]. Impulse value can be identified as a potential index for the damage associated with the buried blast. In general, most of the available literatures on the buried blast focus on the impulse imparted by the sand, but many fail to address the complex dynamics involved during the sand outburst.

Bergeron et al. [2] studied in detail the ejecta flow characteristics by using a high speed x-ray photography. The process involved in the various stages of the buried explosion is outlined below [2,22]:

Blast interaction phase: Upon blast explosion, shock wave is transmitted into the surrounding medium which generates stress waves (compressive) in the soil.

Bubble expansion phase: When the compressive wave reaches the surface, it reflects back as tensile wave (rarefaction wave). This tensile wave combines with detonation products and breaks open the surface of the soil, leading to a bubble formation with a hemispherical shaped soil cap.

Soil ejecta phase: The soil cap eventually collapses followed by the expansion of the soil ejecta in the shape of an inverted cone.

In a more recent study, as an alternate to conventional experiments using explosive charge, McShane et al. [18] developed a scaled buried charge simulator (BCS). The BCS was found to be successful in generating the second and third phase of buried blast, which involves dynamic flow of the sand. However, it is uncertain as to whether the first phase was considered in the simulator. The simulator was operated by a sudden release of the compressed nitrogen gas from a large cylindrical chamber (80 mm long) to a smaller chamber (20 mm long) and then to the sand layer. A CFD analysis (using Ansys–Fluent) was performed for the above mentioned test configuration. It was found that neither shock wave nor blast wave was formed at the exit of smaller chamber. Hence, the blast simulator would ideally generate high pressure gas flow, without a shock front. This exhaust gas flow disperses the buried sand and forms a sand scatter over the surface. BCS has failed to incorporate the interaction of a blast wave with the sand deposit. Also, experiments performed by McShane et al. [18] were considered very close to the sand surface (DoB = 15 mm–30 mm).

The present study aims at developing a similar test facility by accommodating a shock tube in the test assembly. The shock tube is capable of generating wide range of blast waves, representing a near-ideal explosion [23]. The sand ejecta phenomenon is analyzed over large burial depths. The present study also aims at examining the wave propagation in and around the blast source, which would reveal the attenuation behavior of the sand and its influence over crater formation. Peak pressure measurements are obtained using fast response pressure transducers, while the impulse is measured using a vertical impulse pendulum.

1.1. Objectives

The objectives of the present study are: a) to develop an experimental facility using compressed gas-driven shock tube, to generates a buried blast loading condition, b) to obtain the pressure-time response in the sand deposit during blast wave-sand interaction, c) provide qualitative and quantitative insights of the sand ejecta mechanism and d) to carry out a parametric study by varying the depth of burial (DoB = 32 mm–64 mm) and also to assess the target response (pressure and impulse) over a range of stand-off distances (SoD).

2. Overview of shock-driven sand test facility (SSTF)

A schematic diagram of the shock-driven sand test facility (SSTF) is shown in Fig. 1. The major components of the test facility includes: (1) shock tube, (2) cylindrical sand chamber and (3) instrumentation (pressure transducers and impulse measurement device). A blast wave with a spherical shock front radially emanates from the open end of the shock tube into the sand bed, driving the sand particles out of the sand chamber. A detailed description of each component of the shock-driven sand test facility is outlined below.

2.1. Shock tube

Shock tube is a simple laboratory device used to generate shock waves and blast waves. In the present study, a compressed gas-driven shock tube is designed to generate pressure loading identical to the blast wave profile. A typical blast wave is characterized by a leading shock front with a peak overpressure followed by an exponential decay. The two main components of a shock tube are driver

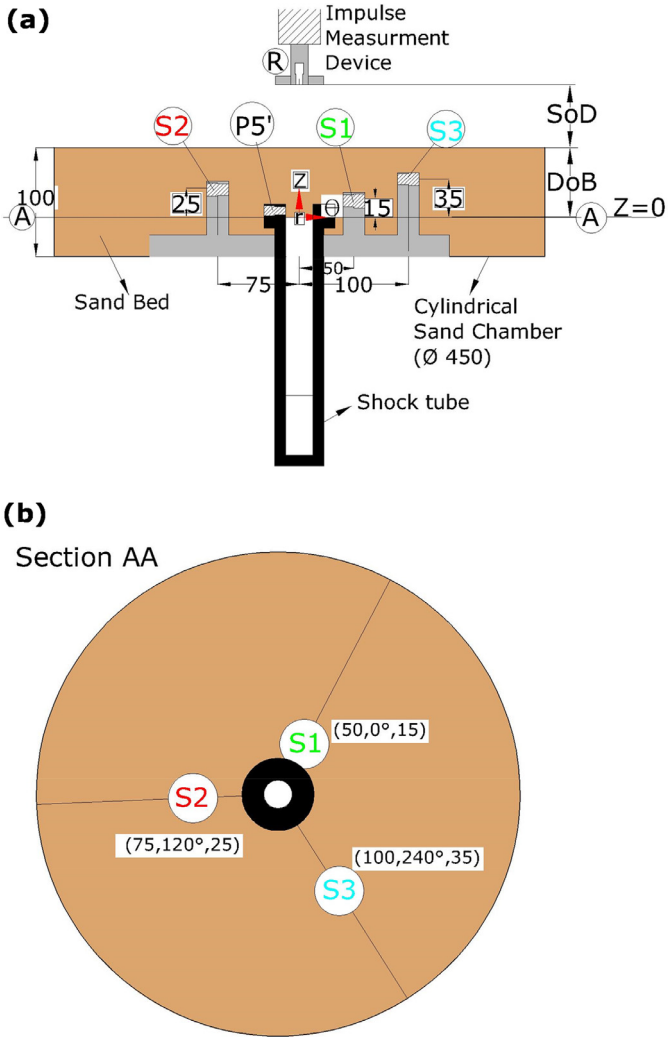

Fig. 1. A schematic overview of the shock-driven sand test facility. (a) cross section view of the simulator, showing the position of the buried sensors for DoB 64 mm and (b) the plan view of section AA. (All dimensions given are in mm and the cylindrical co-ordinate origin is along the axis of shock tube, intersecting with section AA).

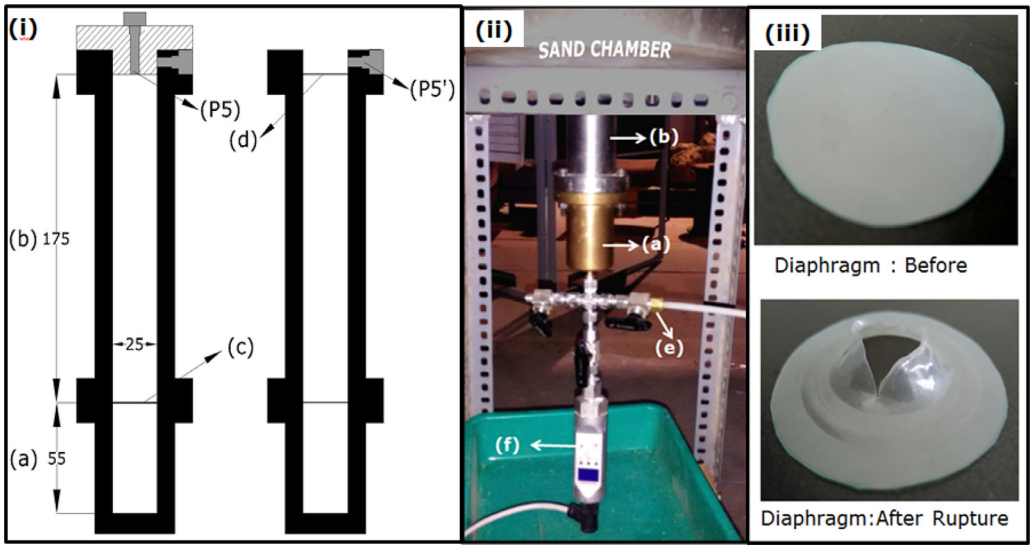

Fig. 2. Shock tube assembly: (i) schematic diagram of the shock tube, (ii) photograph of the assembled shock tube below the sand chamber and (iii) Mylar® diaphragm before and after rupture. (a) driver section, (b) driven section, (c) primary diaphragm, (d) secondary diaphragm, (e) inlet for the high pressure gas and (f) digital pressure gauge. (All dimensions are in mm).

(high pressure) and driven (low pressure) sections, which are separated by a diaphragm. The high pressure gas (nitrogen or helium) is used to pressurize the driver section until the diaphragm ruptures, while maintaining the driven section at low pressure. As the diaphragm ruptures under predetermined pressure conditions, a series of compression waves propagate into the driven section, which coalesces to form a shock wave. Subsequently, an expansion wave travels in the reverse direction of shock wave and gets reflected from the driver section end [24]. Expansion waves eventually catch up with the shock front and decays the pressure level to form a blast wave. Response time of the expansion waves is significant in the formation of the blast wave. A blast wave of desired strength can be created by varying the thickness of the diaphragm or by choosing a lighter driver gas (helium) or by decreasing the pressure of the gas in the driven section. For all the experiments in present study, helium is used as driver gas and the driven section is kept at atmospheric pressure and room temperature.

A schematic diagram of the shock tube considered in the SSTF is shown in Fig. 2i. The length of the driver section is 55 mm (a) and the driven section is 175 mm long (b). Both the sections are manufactured using stainless steel (SS 304) with an internal diameter (ID) and external diameter of 25 mm and 50 mm respectively. An assembled shock tube setup is shown in Fig. 2ii. The driver section is connected to the high pressure helium cylinder using a flexible hose (e). The diaphragm rupture pressure is recorded from the digital gauge (f) (Barksdale Inc. SW2000 pressure switch). The shock tube is provided with two diaphragm mounting sections, primary diaphragm separating the driver and driven sections and the secondary diaphragm separating the driven section and the sand chamber. Mylar® sheet (polyester film) of thickness 0.1 mm (shown in Fig. 2iii) is used as the primary diaphragm (c) and a tracing paper (60–65 GSM) is used as the secondary diaphragm (d). The thickness of paper diaphragm is chosen such that it has minimum effect on the blast wave profile and the paper also has to withstand the overburden pressure exerted by the sand. In order to record the generated blast wave, the open end of the driven section is closed by a flange with an embedded piezoelectric pressure sensor, P5 (PCB 112A22). A typical blast wave signal recorded from the P5 pressure sensor of the shock tube is shown in the Fig. 3. The peak reflected pressure is found to be 23.75 ± 0.5 bar and the positive phase duration is measured to be 475 ± 25 μs. In the SSTF, pressure sensor P5′ (PCB113A24) is located on the driven section just above the paper diaphragm (refer Fig. 2i), to record the in-sand blast pressure (upon rupturing the paper diaphragm). For the sake of ease in representation, all the pressure values in this paper will be represented in unit of bar ($1\ \text{bar} = 10^5\ \text{N/m}^2$).

Shadowgraph technique is used for the visualization of the blast wave. Fig. 4 shows the shadowgraph image of the blast wave emerging from the open end of the shock tube (without overburden sand). A leading hemispherical shaped shock front is followed by a turbulent plume of compressed gas mixture (helium and air) along with the ruptured pieces of the paper diaphragm. The speed of the blast wave in the open atmosphere is supersonic (Mach number > 1) travelling at a velocity of 375 m/s. The blast wave generated is considered to be of low-moderate strength, with relatively low driving pressure (behind shock front). The hemispherical blast wave profile closely resembles that of any open field explosion on a semi-infinite medium (earth).

2.2. Test bed preparation

The sand test chamber has a capacity to prepare a sand bed of depth of 100 mm and 450 mm of diameter. A larger diameter of the test bed is chosen such that the boundaries had no influence on the wave propagation and the crater width. The shock tube assembly is connected underneath to the sand chamber, such that the blast wave exits into the sand chamber. Different DoB cases are

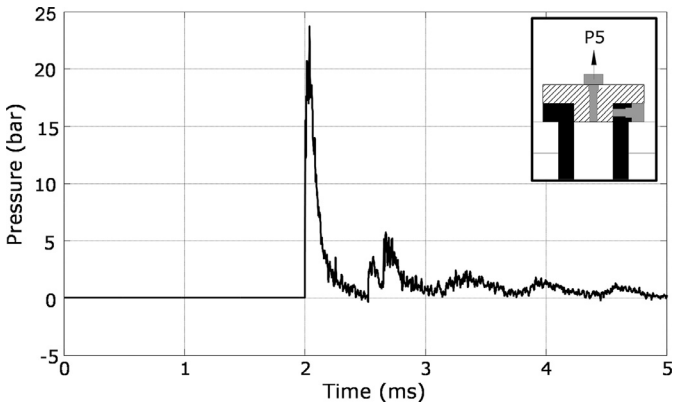

Fig. 3. Pressure–time curve recorded (P5) at end of the shock tube.

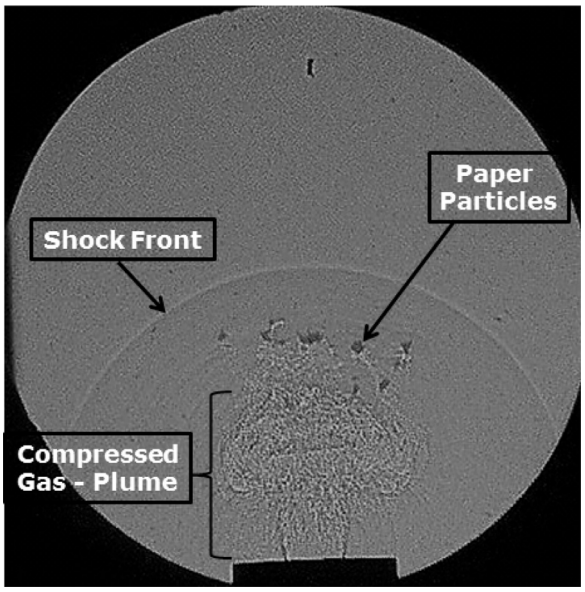

Fig. 4. Shadowgraph image at the open end of the shock tube.

constructed by using appropriate spacer bars to position the shock tube end.

Dry river bed sand is used in the present study. The sand is completely oven dried at 130° C and subsequently air dried for 24 h. The grain size of sand varies from 0.075 mm to 2.36 mm and is classified as 'poorly graded' with symbol SP as per Unified Soil Classification System (USCS). The grain size distribution of the sand particle is obtained by performing a dry sieve analysis test. The gradation property of the sand is listed in Table 1 and the grain size distribution curve is shown in Fig. 5.

Prior to each experiment, a sand bed of 100 mm depth is prepared by using sand pluviation technique. The sand pluviation apparatus consist of a fixed overhead hopper, which is in turn connected to a flexible, adjustable (100–500 mm in height) PVC pipe. The bottom end of the PVC pipe is connected to a sand diffuser. The sand diffuser is a hollow cylindrical pipe of 100 mm in length, with a 60° inverted cone welded to the opening end. In short, the sand particles are poured into the hopper; the sand passes through the PVC pipe and disperses out of the diffuser. The diffuser is moved to and fro such that the sand that exit from the conical surface is uniformly distributed in the chamber. A constant sand flow rate is thus achieved and the density is relatively kept constant by maintaining a constant height of fall. Such a method will help in delivering repeatable sand layer deposits over a large area. The height of fall determines the desired relative density of the sand deposit [25]. Height of fall is defined as the distance between the top of the sand bed to the bottom of the sand diffuser (base of the cone). In the present study, the sand bed is prepared with an approximate relative density of $45 \pm 2\%$ which corresponds to dry density of $1566 \pm 20\ kg/m^3$. The relative density of the sand deposit is monitored by placing small cups of known volume at different location in the sand chamber [26].

Table 1
The gradation properties of the sand.

Parameter	Quantity
D10 (mm)	0.26
D50 (mm)	0.7
Coefficient of uniformity, C_u	3.07
Coefficient of curvature, C_c	0.96
Maximum void ratio, e_{max}	0.9
Minimum void ratio, e_{min}	0.53

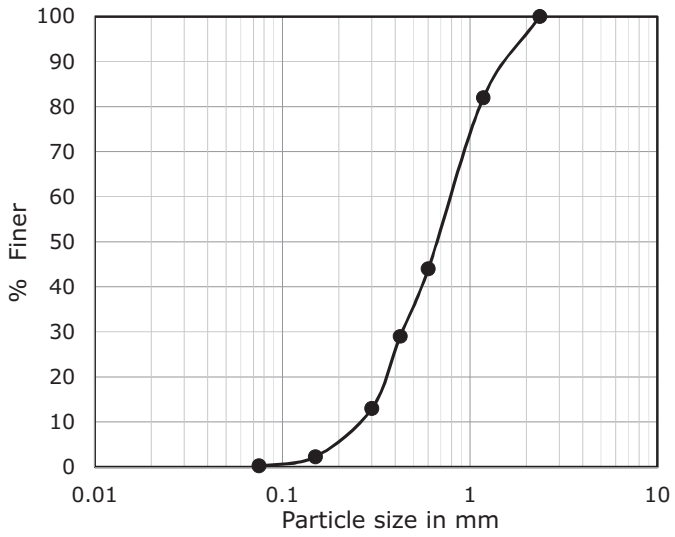

Fig. 5. Grain size distribution curve for the sand used in the present study.

2.3. Instrumentation

2.3.1. Piezoelectric pressure transducers

In order to measure the pressure-time response around the blast, three piezoelectric pressure transducers (PCB 113 Series) are embedded inside the sand bed. The three transducers are spaced apart 120° to each other and radially increasing at an offset of 25 mm in radius from the ID of the shock tube. All the pressure signal data are captured with a sampling rate of 500 kHz using a DL750 Yokogawa scope recorder. In addition, pressure signal is also measured at the exit of the shock tube (P5′). The schematic diagram displaying the position of the transducers, S1 (PCB 113B23), S2 (PCB 113B22), S3 (PCB 113A24) and P5′ (PCB 113A24) are shown in the overview diagram of the shock-driven sand test facility (Fig. 1). A photograph of embedded transducers in the sand chamber is shown in Fig. 6a. The transducers arrangement is ensured to record the spherical outward movement of the blast wave.

In order to measure the peak pressure of the sand discharge, a transducer R (PCB 113B23) is mounted on a rigid target frame. The target frame is placed at varying SoDs and aligned such that the sensor is pointing towards the center of the buried shock tube. The pressure measured by sole transducer 'R' is expected to be highly localized and includes the pressure exerted by both the gas cloud and the particle impact. However, this peak pressure value will give an indication of total pressure imparted to the targets upon buried blast loading.

Subsequently, impulse imparted to the fixed target is calculated from the pressure-time data recorded by transducer R, using Eq. (1). Where, t_1 is the positive pressure phase duration, it is time duration between the rise of pressure and the end of the first positive pressure phase with absolute pressure of zero. The photograph of the rigid frame along with the transducer 'R' is shown in Fig. 6b. Measuring impulse from the localized pressure data might not be accurate enough. In order to obtain more reliable data, the impulse measurements are also carried out using a simple impulse pendulum.

$$I = \int_0^{t_1} P(t)dt \tag{1}$$

2.3.2. Vertical impulse pendulum

The vertical pendulum is made up of two components, linear bearing and a piston. The linear bearing is fixed firmly into the solid cylindrical block which is in turn bolted to the rigid target plate. The linear bearing is provided with anti-friction stainless steel ball

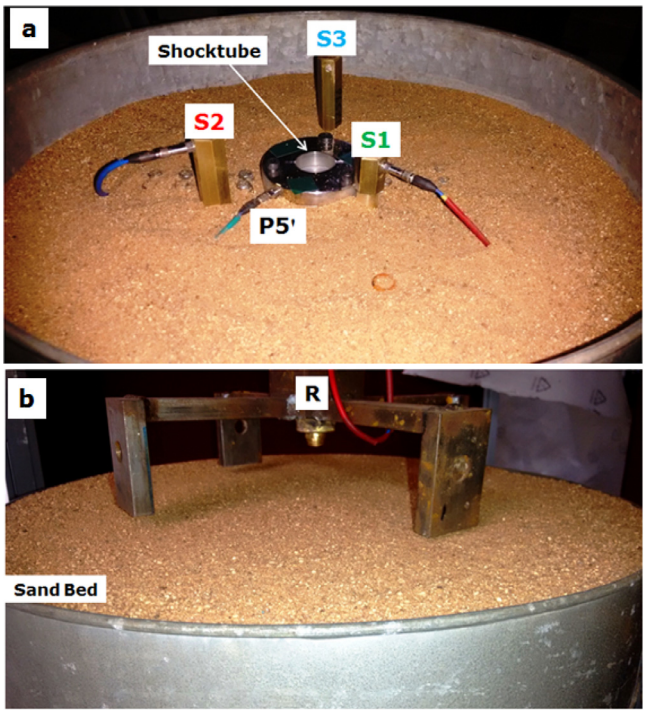

Fig. 6. A photograph of the sand bed chamber showing the positioned pressure transducers (a) buried sensors (b) overhead sensor.

bushings. The cylindrical shaft of the piston is inserted into the linear bearing, such that the circuit balls in the bearing comes in rolling contact with the shaft. The shaft is made up of hardened steel (SS 440), coated with ceramic aluminum alloy, making it an ideal surface finish with least coefficient of friction. The shaft travels axially back and forth along the bearing. The upper end of the shaft is clamped with a c-clip and the bottom end is connected to cylindrical piston head. For ensuring repeatability, all the experiments are carried out with two different piston mass, 0.634 kg and 0.534 kg. The height of the target frame is varied axially with the help of a vertical actuator (with an accuracy of 1 mm). The pendulum assembly is aligned and centrally placed along the axis of the shock tube with the piston head placed at a SoD from the top surface of the sand bed (Fig. 7).

When the sand ejecta strike the piston head, the momentum is transferred to the piston head. The piston accelerates upward attaining a maximum height and then decelerates due to gravity. The maximum vertical displacement (h_a) of the pendulum is captured using a high speed camera (Phantom V710 with Nikon 70–210 mm lens; images are captured with an exposure of 90 μs at 11,000 frames per second). The maximum impulse (I_{max}) imparted to the pendulum is calculated from Eqs. (2) and (3). Where, V_j is the velocity of the piston, g is the gravitational constant (9.8 m/s^2) and m_p is the total mass of the piston head plus shaft.

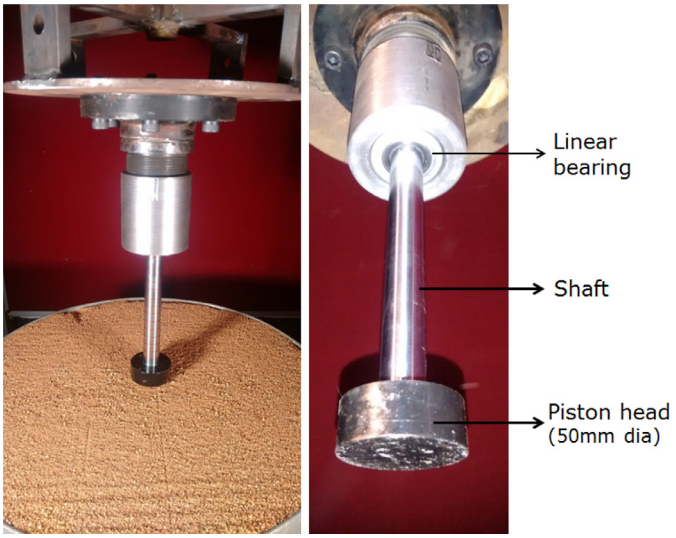

Fig. 7. A photograph of the vertical impulse pendulum.

$$V_j = \sqrt{2gh_a} \tag{2}$$

$$I_{max} = V_j * m_p \tag{3}$$

2.4. Operation of the test facility

The experimental test series can be classified into three sections based on the objectives: (1) blast wave-sand interaction phenomenon is studied for three DoB cases (32 mm, 48 mm and 64 mm), (2) dynamics of sand ejecta is analyzed for the same DoB cases. (3) Impulse and pressure measurements are carried out by varying SoDs (40 mm, 80 mm, 120 mm, up to 240 mm) for different burial depths (DoBs).

As outlined in the previous section, the components of the SSTF are assembled together and placed on a level ground surface. The primary diaphragm (Mylar®) and the secondary diaphragm (paper) are held in position with the help of the fasteners, ensuring leak proof conditions. The sand bed is prepared and surface is levelled using a flat edge. The experimental setup is illuminated using four high powered halogen lamps (500 W), which serve as light source for the high speed camera. The shock tube is operated by rupturing the Mylar® diaphragm. A blast wave is formed in the shock tube and travels further into the sand deposit by rupturing the paper diaphragm. Subsequently, the camera and pressure transducers are triggered (by P5′ signal), the visual and voltage measurements are recorded. Similar experimental procedure is carried out for different combinations of DoBs and SoDs. Kindly note, for the experiments involved with the diagnosis of sand ejecta, the embedded sensors (S1–S3) are removed and all the experiments are performed minimum twice to ensure test repeatability.

3. Experimental results

3.1. Pressure versus time response around blast-sand interaction

The pressure (stress) variation recorded by the buried transducers, P5′, S1, S2 and S3 for three DoB cases is shown in the Fig. 8. The P5′ signal corresponds to the in-sand pressure measurement, a peak overpressure of about 14 bar with a positive phase duration of 1.5 ms is recorded immediately at the exit of shock tube. Though the peak pressure amplitudes obtained are significantly lower when compared to Bergeron et al. [2], the blast wave features of P5′ descriptively matches well with their ground shock pressure profile.

The energy released from the blast wave-sand interaction is transmitted either as shock wave or stress wave into the surrounding sand medium. The formation of shock wave or stress waves in the medium depends on the intensity of the blast wave (energy released) and the acoustic impedance of the medium (for propagation). For all three DoB cases (Fig. 8), a well-defined shock front is identified very close to the shock tube exit (P5′). As the shock front propagates through the sand, it attenuates with distance and reduces to low intensity stress wave. Referring to Fig. 8a and b, two distinctive events are observed over a period of 6 ms, the first event includes the passage of the stress wave, marked by the presence of initial pressure peak (see S1 signal in inset Fig. 8a and b). Under these conditions, the stress wave further traverses vertically and disturbs the surface of the sand bed. This event is captured using high

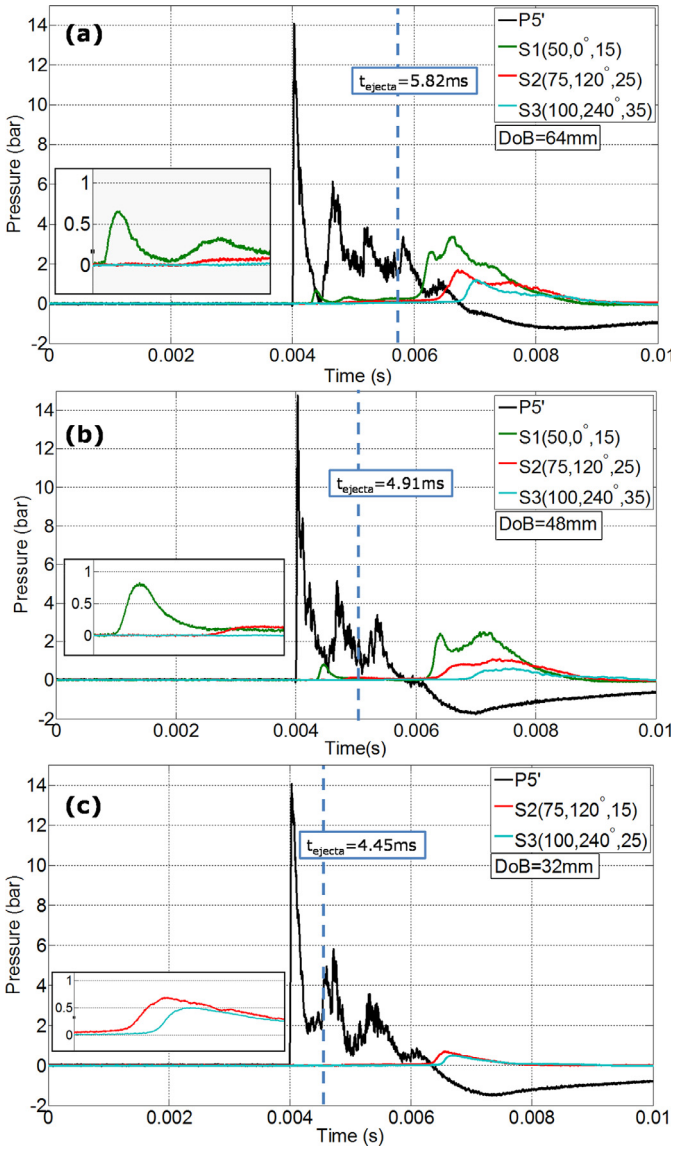

Fig. 8. Pressure–time curve of gauges P5′, S1, S2 and S3 recorded for three different cases: (a) DoB = 64 mm, (b) D0B = 48 mm and (c) DoB= 32 mm, S1 adapter is below the burial depth, thus only S2 and S3 signals are shown. P5′ signal is used as trigger signal. (Inset Fig. : enlarged portion of the initial peaks).

speed camera and the time of initiation of surface disturbance is displayed as a dotted line (t_{ejecta}) in Fig. 8. The radially attenuating stress wave has diminished across transducers S2 and S3. Meanwhile, the second event begins with the expansion of the compressed gaseous product (mixture of helium and air). Three distinctive peaks of S1–S3 are observed with gradual rise to the peak and decreasing over a long period (termination of the event). The pressure amplitude of the second event is found to be larger than those associated during the first event (similar trends were numerically observed by Tan et al. [14]). Further observing the initial period of the signal, there is no trace of the rarefaction wave from the surface. It is believed either the intensity of the wave is too low, or the wave effect is suppressed by the outgoing gaseous expansion.

3.2. Sand ejecta

The images of the sand ejecta, captured using high speed camera are shown in Fig. 9–11. The figures also show the projection contours of the sand outburst. The contour plots are generated by using image processing technique available in Matlab. Sobel edge detection algorithm is used with a threshold value of 0.1. If the pixel gradient value is lower than this threshold, it is consider to have broken edges or noises [27]. The abscissa of the contour plot represents the diameter of the top surface of sand bed and the ordinate shows the vertical position of the dispersed sand particles.

The important parameters which influence the pattern of the ejecta are the confinement effect and the depth of burial. The sand discharge experiments are carried out for three different DoB cases. Referring to 32 mm DoB case (Fig. 9), an expanding gas sphere accelerating outwards from the surface is observed at 2.5 ms (termed as 'bubble expansion' by Bergeron et al.1998). Further, the bubble slowly begins to collapse giving way to the sand particles. The inherent cohesion between the particles is lost with the increase in ordinate length and the sand particles emerge out in a radial pattern (termed as 'expanding inverted cone' by McShane et al. [18]). In addition, dome-cap like formation is observed from $t = 10.1$ to 15.3 ms, which has traversed all along the axis of the chamber. It is this portion of the sand ejecta, placed immediately above shock tube that carries the maximum momentum. The sand density around the dome-cap is considerably higher compared to the other region of the radial cone. After a certain period ($t > 20$ ms), as the driving pressure gradually drops, sand dispersion reduces with time and eventually falls down due to gravity. The amount of sand ejected out of the sand chamber leads to the formation of a crater. A 183 mm circular disk shaped crater is formed, which has perfectly centered itself to the opening of the shock tube.

Further experiments are carried out by increasing the overburden sand thickness. Similar contour plots and images are captured at specific intervals, shown in Figs. 10 and 11 for the DoB cases of 48 mm and 64 mm respectively. The same initial test conditions are reproduced. By comparing the contours of Figs. 10 and 11 with Fig. 9, there are significant changes in the pattern of the ejecta. For instance, the presence of the inverted cone like structure is replaced with a cylindrical column of sand. The increase in the confinement has restrained the sand from expanding radially; instead the sand is directed vertically upwards. Noticeably, there is well defined dome-cap ejecting out of the cylindrical formation. However, unlike the dome-cap seen isolated in Fig. 9, the dome-cap in Figs. 10 and 11 is attached to the cylindrical formation. As the DoB increases, zone of influence of the outgoing pressure disturbance encompasses large volume of the sand, resulting in higher sand mass flow out of the test bed. However, the driving pressure of the gaseous products being constant, limits the flow rate of the sand. As a result, a dense annular region is formed at the base of the cylindrical column and large amount of the sand is dispersed out leaving behind huge cavity. The crater dimension for 48 mm and 64 mm DoB are 235 mm and 310 mm respectively, and the crater slope is found to be steeper compared to 32 mm DoB.

The velocity of the ejecta is calculated from the contour plots. Successive high speed images captured at an interval of 90 μs are compared by measuring the distance travesed by the apex of the dome-cap. The velocity of the ejecta is found to increase from the bubble expansion phase to the dispersion phase. The greater part of the momentum is considered to be transferred from the bubble expansion to the dome-cap of the ejecta. In all the three cases, a clear well defined dome is formed between Y intercept of 100 and 200 mm. As a reference, the velocity measurements are made between Y-intercept of 125 mm and 425 mm. Interestingly, for DoB of 32 mm, the velocity is found to be almost constant (mean velocity, $v_x = 26.32$ m/s with standard deviation, $\sigma_x = 0.144$). The 48 mm DoB test resulted in velocity ranging from 18.07 m/s to 21.31 m/s ($v_x = 19.71$ m/s, $\sigma_x = 1.06$) and lastly, the velocity range for 64 mm DoB is from 7.94 m/s to 11.33 m/s ($v_x = 9.94$ m/s, $\sigma_x = 1.3$). From the trend of the velocity data, it is evident that there is clear reduction in the velocity as the DoB is increased. These data also infer, for burial depth close to the top sand surface (32 mm), the dome-cap

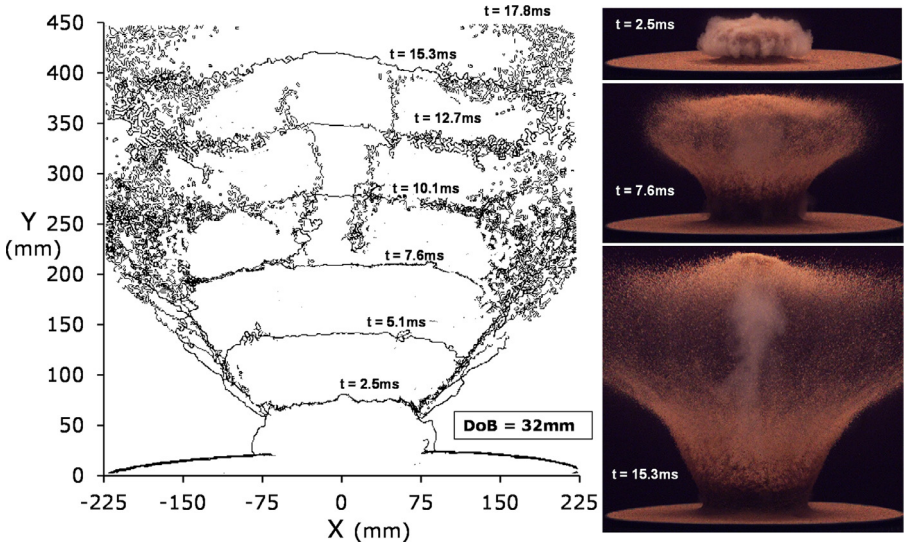

Fig. 9. A contour profile of the sand ejecta at different time instance for 32 mm DoB case.

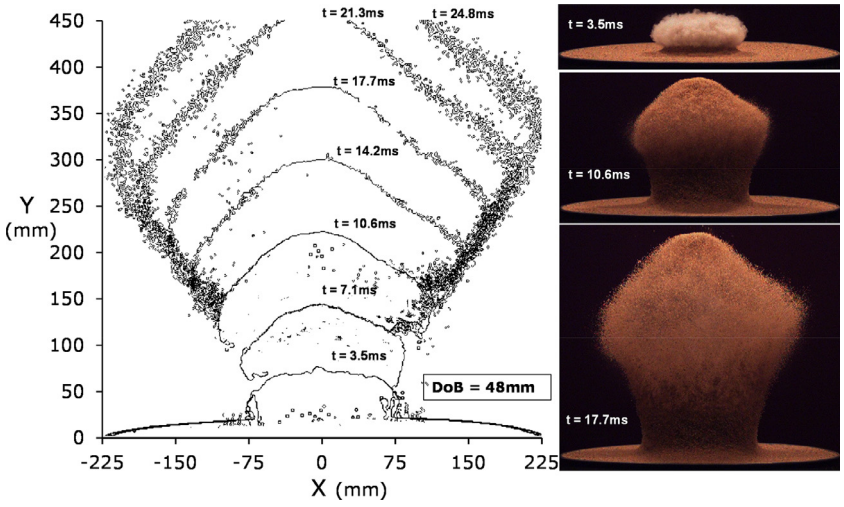

Fig. 10. A contour profile of the sand ejecta at different time instance for 48 mm DoB case.

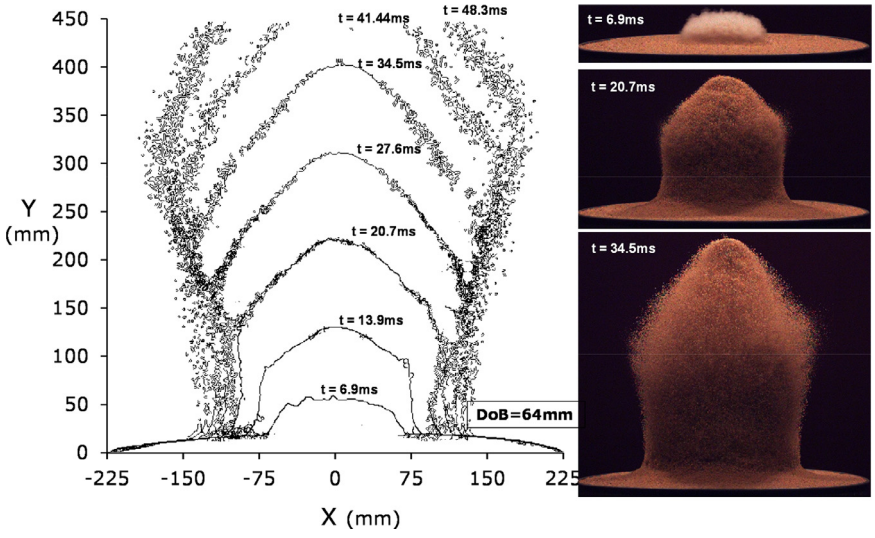

Fig. 11. A contour profile of the sand ejecta at different time instance for 64 mm DoB case.

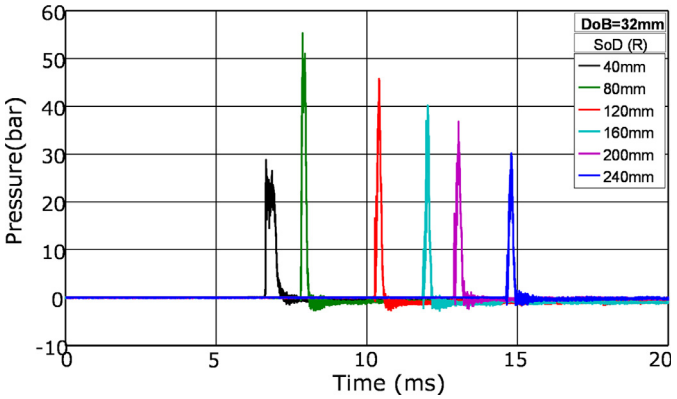

Fig. 12. Pressure–time curve of overhead sensor R for SoDs varying from 40 mm to 240 mm for DoB of 32 mm.

isolates itself from the rest of the sand ejecta and travels at a constant velocity.

3.3. Pressure and impulse measurement

3.3.1. From pressure transducers on rigid target

The pressure measurements recorded from the overhead transducer 'R' for the 32 mm DoB case is shown in Fig. 12. By keeping the DoB constant, the height of rigid target frame is increased with an incremental SoD of 40 mm. The pressure-time history for different SoD, shows similar distinctive spike like structures. The spikes are attributed to the impact loading by the dome-cap. The signals are characterized by a sharp rise, followed by a sudden drop. The maximum peak pressure is observed at SoD of 80 mm. At lower SoD (40 mm), the peak pressure is found to be lower and drops off at a steady rate with increase in the positive phase duration. The partial formation of the dome-cap with relatively low impact velocity can be accounted for to the low pressure value. For the test cases with SoD greater than 80 mm, the peak pressure is found to decrease linearly with increase in the SoD.

The impulse calculated from the recorded pressure signals for the 32 mm DoB case is shown in Fig. 13. Two repeated test measurement data are plotted and a trend line is drawn by taking an average between them. There is a gradual decrease in the impulse value with the increase in SoD. Similar pressure and impulse trend were observed by McShane et al. [18] for smaller depth of burial conditions. However, a single transducer placed at the target may not accurately predict the imparted impulse.

3.3.2. From vertical pendulum

The vertical impulse pendulum outlined in Section 2.3 is used to measure the impulse imparted to the target. The impulse transferred to the target includes the effect due the dome-cap, the gaseous mixture and the sand debris of the ejecta. Fig. 14 is provided with the impulse data for all the three DoB cases, with increasing SoD (40 mm–120 mm). For SoD larger than 120 mm, the sand debris completely masks the pendulum obstructing the field of view of the camera. The impulse value is averaged between the two experimental test results of different piston mass. As expected, the impulse measured from the pendulum is found to be notably lower than the measurement made using the transducers.

The impulse imparted to the pendulum is observed to decrease with the increase in the stand-off distance (as observed in the transducer method for 32 mm DoB). Further, maximum impulse is observed when the target is closer to the sand surface, perhaps because of the presence of the 'bubble expansion' cloud. For a target placed at a SoD of 80 mm, the maximum impulse is observed for the DoB of 32 mm and similarly for a target placed at 120 mm the maximum impulse is found when the DoB is 48 mm. It is interesting to note that, the maximum impulse transfer for a specific SoD, is observed when SoD/DoB value is equal to 2.5. It seems reasonable to state the following hypothesis. When the ratio of SoD to DoB equals 2.5, the ejecta has consumed optimum crater volume to create a well-defined dome-cap. This dome-cap is coerced with utmost velocity (by gaseous products) to impart maximum impulse to the target. Further, experiments show a decrease in the momentum with increase in the overburden sand depth ($>$ 50 mm). This effect is termed as camouflet condition [2], where the blast wave and the gaseous products are completely contained by the sand.

3.4. Discussion

In the present study, we have used compressed gas-driven shock tube to generate blast wave in the sand deposit. In this section, we will present and compare the experimental results (peak overpressure) with the available data in the existing literature on the buried

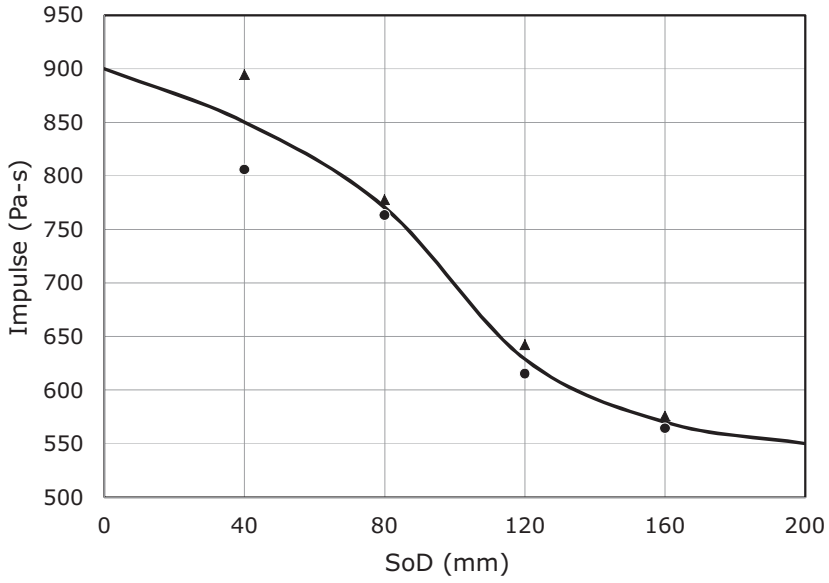

Fig. 13. Variation of the impulse with the SoD for 32 mm DoB case.

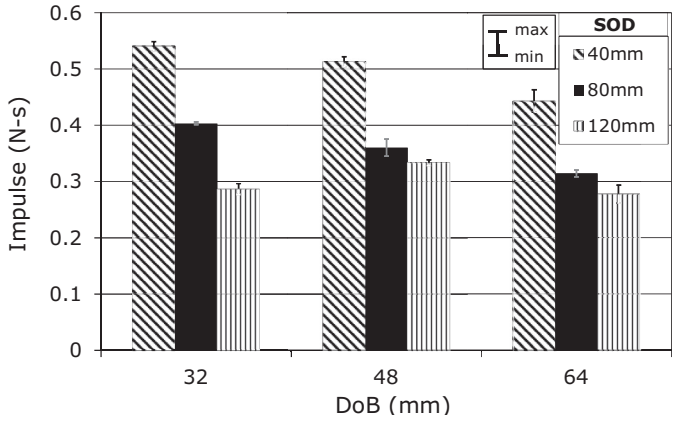

Fig. 14. Variation of the impulse with the SoD for different DoB. (max. and min. values are shown within the standard bars).

landmine experiments (operated by using explosives). However, a direct comparison of experimental efficacy is not possible, due to the variability in the different parameters of the test conditions. Bergeron et al. [2] and Roger [12] performed buried explosion study using 100 g of C4 explosive, subsequently peak pressure data were recorded both below (in-sand) and above (in-air) the sand surface. The pressure measurements above the surface were done all along the center of the buried charge, while the buried sensors were located deep below the source of detonation (Refer [2] and [12] for exact location). Although the recording of the buried sensors of Bergeron et al. [2] and Roger [12] was not captured around the buried charge, their data can provide quantitative information on the pressure levels in sand and the stress waves generated by the detonation. In Fig. 15 we compare the results from the literature to the pressure data recorded in the present study. When analyzing the peak pressure values with the existing data, the pressure measurements made above the sand surface is observed to have a similar range and shows a consistent trend with the increase in the SoD, confirming the validity of the present experiment. On the contrary, the peak pressure values in the sand are found to be significantly lower when compared to the tests performed using explosives. In fact, the present experimental values are off by an order of magnitude. Further, the velocities of cloud expansion are much lower than those found in the case of Bergeron et al. [2]. As a consequence, it is believed that pneumatically generated blast pressure is insufficient to create the effects of actual buried explosion in sand. The effects include the presence of shock front in the sand medium, high compression followed by rapid decompression, particle breakage and crushing, and the thermal radiation resulting from the detonation. However, examining the sand ejecta characterization results confirms that shock tube based tool enables us to study later stages of buried explosion, the physical sand ejecta impact on the overlying targets. Hence, the present study is limited to the study of the dynamics involved during sand ejecta and assesses the resulting impulse transfer, induced by relatively low driving pressure of the blast wave. The buried blast events can be simulated within laboratory environments using a shock tube, the main limitation is the inability of the compressed gas-driven shock tube to generate blast wave of high pressure. However, a detonation-driven shock tube can possibly overcome this limitation.

4. Summary and conclusion

A laboratory scale shock-driven sand test facility is developed to deliver a blast wave, below the buried sand layers. The experiments have been performed using dry cohesionless soil at three different burial depths (DoB), 32 mm, 48 mm and 64 mm. Initial set of experiments carried out in the compressed gas-driven shock tube, ensured smooth transmission of blast wave of moderate strengths driven by compressed gases. The shock tube is operated with a relatively low driving pressure of compressed helium gas, to generate a sand-blast overpressure of about 14 bar at the DoB level. The experiments are primarily designed to investigate the sand ejecta kinematics during

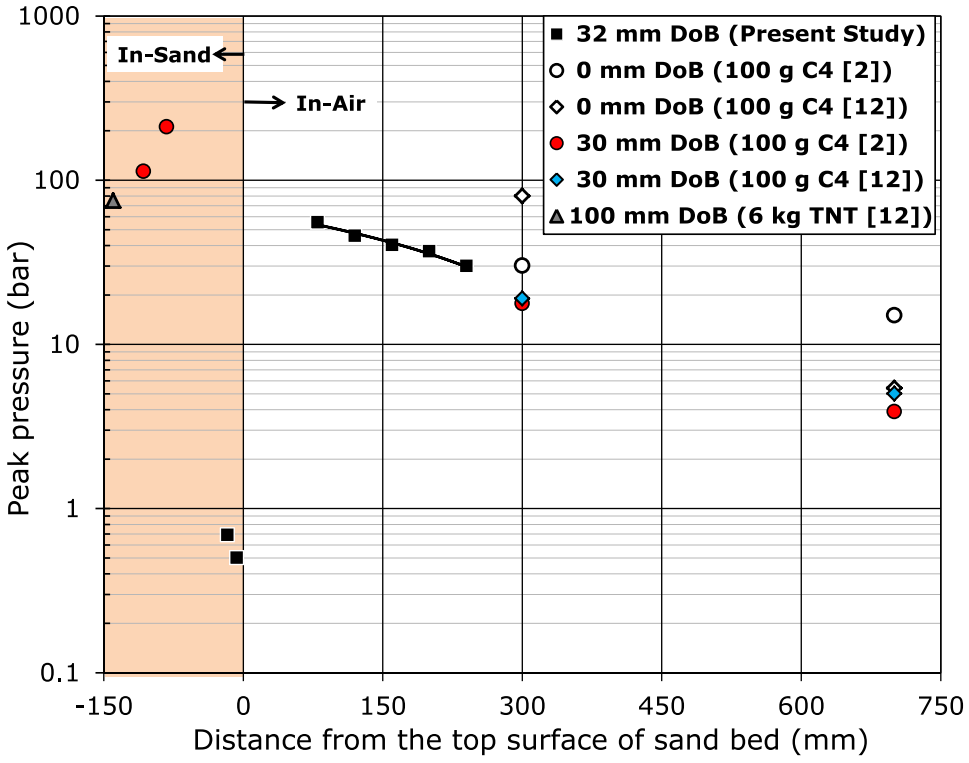

Fig. 15. Comparison of the results from the present work with the results of experiments associated with landmine detonation [2,12].

blast wave interaction with the sand media and also to assess the variability of the imparted impulse with the burial depth.

Dynamic wave propagation and the pressure distribution around the blast source have been studied, upon blast wave-sand interaction. Stress waves attenuate significantly in the sand deposit and the peak pressure induced by the stress wave is much smaller than the rise in pressure generated by the gaseous products (mixture of compressed gases). Moreover, decayed stress wave is too weak to cause any significant changes to the sand ejecta phenomenon. This justifies the fact, the sand ejecta is predominantly caused by the expansion of the gaseous products. The peak pressure and impulse measurements are made using transducers and vertical pendulum respectively, at varying SoDs. The peak pressure values are found to be sensitive to the impact of the ejecta's dome-cap. The depth of burial has a greater influence on the amount of impulse transmitted to the target. For all the DoB cases considered, maximum impulse is found when the stand-off distance is relatively small (40 mm), which could be due to the sustained pressure around the bubble envelope. For SoD considered further away from the zone of bubble expansion, the impulse transmitted is mostly governed by the sand ejecta and a maximum value is achieved when the SoD/DoB is 2.5. The results obtained in this paper also indicate that the crater dimensions (radius and the slope) increase with the increase in DoB (upto 64 mm).

The aim of this study is not to compare with real explosion, but to develop a laboratory environment for studying buried impact or blast loading mechanism. The study has attempted to experimentally characterize the different phases involved in the sand ejecta, during the interaction of blast wave with sand, followed by expansion of the driving compressed gas. Since the conditions in the shock-driven sand facility is well-controlled and are equipped with advanced monitoring and diagnostic techniques, this would enable us in qualitative understanding of the behaviour of sand during buried blast loading. Further studies are needed to conclusively demonstrate the shock tube based tool in simulating actual buried blast explosions.

Acknowledgement

The experiments were performed at Laboratory for Hypersonic and Shock Wave Research (LHSR) at Indian Institute of Science, Bangalore. The authors acknowledge the efforts of colleagues and non-technical staffs in LHSR and Soil Mechanics Laboratory, at Indian Institute of Science. The work is supported by grants provided by DST, Govt. of India and International bi-lateral co-operation division, Indo-German (DST-BMBF) cooperation in civil security research (F. No. IBC/FR6/BMBF/CSR/R-03/2015).

References

[1] Cheeseman BA, Wolf S, Yen CF, Skaggs R. Blast simulation of explosives buried in saturated sand. Fragblast 2006;10(1–2):1–8.
[2] Bergeron D., Walker R., Coffey C. Detonation of 100-gram anti-personnel mine surrogate charges in sand - a test case for computer code validation. Suffield Report No. 668. Ralston, Alberta, Canada: Defence Research Establishment Suffield; 1998.
[3] Bergeron DM, Tremblay JE. Canadian research to characterise mine blast output. In: 16th international symposium on the military aspects of blast and shock; 2000.
[4] Fourney WL, Leiste U, Bonenberger R, Goodings D. Explosive impulse on plates. Fragblast 2005;9:1–17.
[5] Taylor LC, Skaggs RR, Gault W. Vertical impulse measurements of mines buried in saturated sand. Fragblast 2005;9:19–28.
[6] Fox DM, Huang X, Jung D, Fourney WL, Leiste U, Lee JS. The response of small scale rigid targets to shallow buried explosive detonations. Int J Impact Eng 2011;38(11):882–91.
[7] Pickering EG, Steeve ChungKimYuen, Nurick GN. The influence of the height of burial of buried charges - some experimental observations. Int J Impact Eng 2013;58:76–83.
[8] Hlady SL. Effect of soil parameters on land mine blast. In: 18th military aspects of blast and shock (MABS) conference, Bad Reichenhall; 2004.
[9] Neuberger A, Peles S, Rittel D. Scaling the response of circular plates subjected to large and close-range spherical explosions. Part II: buried charges. Int J Impact Eng 2007;34:874–82.
[10] Anderson CE, Behner T, Weiss CE, Chocron S, Bigger RP. Mine blast loading: experiments and simulations, Southwest Research Institute Report 18.12544/011; 2010.
[11] Ambrosini RD, Luccioni BL, Danesi RF, Riera JD, Rocha MM. Size of craters produced by explosive charges on or above the ground surface. Shock Waves 2012;12:69–78.
[12] Roger E. Mines buried in dry and saturated soils: blast experiments, soil modeling and simulations, PhD Thesis (HAL Id : tel-01237997). Université Grenoble Alpes; 2015.
[13] Karinski YS, Feldgun VR, Yankelevsky DZ. Shock waves interaction with a single inclusion buried in soil. Int J Impact Eng 2012;45:60–73.
[14] Tan Z, Zhang W, Cho C, Han X. Failure mechanisms of concrete slab–soil double-layer structure subjected to underground explosion. Shock Waves 2014;24(5):545–51.
[15] Braid MP. Experimental investigation and analysis of the effects of antipersonnel landmine blasts 2001 Special Publication, DRES SSSP 2001-188.
[16] Foedinger J. Methodology for improved characterization of landmine explosions. SBIR phase-II plus program, technical interchange meeting. Material Science Corporation; 2005.
[17] An J, Tuan C, Cheeseman B, Gazonas G. Simulation of soil behavior under blast loading. Int J Geomech 2011;11(4):323–34.
[18] McShane GJ, Deshpande VS, Fleck NA. A laboratory-scale buried charge simulator. Int J Impact Eng 2013;62:210–8.
[19] Clarke SD, Fay SD, Warren JA, Tyas A, Rigby SE, Elgy I. A large scale experimental approach to the measurement of spatially and temporally localised loading from the detonation of shallow-buried explosives. Meas Sci Technol 2015;26:015001.
[20] Ehrgott JQ, Akers SA, Windham JE, Rickman DD, Danielson KT. The influence of soil parameters on the impulse and airblast overpressure loading above surface-laid and shallow-buried explosives. Shock Vib 2011;18:857–74.
[21] Clarke SD, Fay SD, Warren JA, Tyas A, Rigby SE, Reay JJ, et al. Geotechnical causes for variations in output measured from shallow buried charges. Int J Impact Eng 2015;86:274–83.
[22] Deshpande VS, McMeeking RM, Wadley HNG, Evans AG. Constitutive model for predicting dynamic interactions between soil ejecta and structural panels. J Mech Phys Solids 2009;57:1139–64.
[23] Courtney EDS, Courtney AC, Courtney MW. Shock tube design for high intensity blast waves for laboratory testing of armor and combat materiel. Def Technol 2014;10:245–50.
[24] Gaydon AG, Hurle IR. The shock tube in high-temperature chemical physics. London: Chapman and Hall Ltd.; 1963.
[25] Vaid YP, Negussey D. Relative density of pluviated sand samples. Soils Found 1984;24:101–5.
[26] Latha GM, Krishna AM. Seismic response of reinforced soil retaining wall models: influence of backfill relative density. Geotext Geomembr 2008;26(5):335–49.
[27] Efford N. Digital image processing. MA: Addison-Wesley, Reading; 2000. p. 164–73.